

SPECTROSCOPIC CONFIRMATION OF TWO LYMAN BREAK GALAXIES AT REDSHIFT BEYOND 7

E. VANZELLA,¹ L. PENTERICCI², A. FONTANA², A. GRAZIAN², M. CASTELLANO², K. BOUTSIA², S. CRISTIANI¹, M. DICKINSON³, S. GALLOZZI², E. GIALLONGO², M. GIAVALISCO⁴, R. MAIOLINO², A. MOORWOOD⁵, D. PARIS², AND P. SANTINI²

¹INAF Osservatorio Astronomico di Trieste, Via G.B. Tiepolo 11, 34131 Trieste, Italy

²INAF Osservatorio Astronomico di Roma, Via Frascati 33, 00040 Monteporzio (RM), Italy

³National Optical Astronomy Observatory, PO Box 26732, Tucson, AZ 85726, USA

⁴Department of Astronomy, University of Massachusetts, 710 North Pleasant Street, Amherst, MA 01003 and

⁵European Southern Observatory, Karl-Schwarzschild Strasse, 85748 Garching bei Munchen, German

Draft version September 16, 2018

ABSTRACT

We report the spectroscopic confirmation of two Lyman break galaxies at redshift > 7 . The galaxies were observed as part of an ultra-deep spectroscopic campaign with FORS2 at the ESO/VLT for the confirmation of $z \simeq 7$ “z-band dropout” candidates selected from our VLT/Hawk-I imaging survey. Both galaxies show a prominent emission line at 9735Å and 9858Å respectively: the lines have fluxes of $\sim 1.6 - 1.2 \times 10^{-17} \text{ ergs}^{-1} \text{ cm}^{-2}$ and exhibit a sharp decline on the blue side and a tail on the red side. The asymmetry is quantitatively comparable to the observed asymmetry in $z \sim 6$ Ly α lines, where absorption by neutral hydrogen in the IGM truncates the blue side of the emission line profile. We carefully evaluate the possibility that the galaxies are instead at lower redshift and we are observing either [O II], [O III] or H α emission: however from the spectroscopic and the photometric data we conclude that there are no other plausible identifications, except for Ly α at redshift > 7 , implying that these are two of the most robust redshift determination for galaxies in the reionization epoch. Based on their redshifts and broad-band photometry, we derive limits on the star formation rate and on the ultraviolet spectral slopes of the two galaxies. We argue that these two galaxies alone are unlikely to have ionized the IGM in their surroundings.

Subject headings: galaxies: distances and redshifts - galaxies: high-redshift - galaxies: formation

1. INTRODUCTION

The recent progress in the exploration of the very early Universe has been quite remarkable with several groups beginning to assemble large samples of candidate high-redshift galaxies ($z > 6.5$). These include narrow-band selected Ly α emitters (LAEs) (Ota et al. 2010; Ouchi et al. 2010; Hu et al. 2010), and color-selected Lyman break galaxies (LBGs) from wide and deep surveys carried out in the near-IR, mainly with WFC3 (Bouwens et al. 2010a; McLure et al. 2010) and Hawk-I (Castellano et al. 2010a; Castellano et al. 2010b, C10a and C10b in the following).

Despite the large number of candidates, spectroscopic confirmation of a sizable sample of high redshift galaxies is still lacking. A systematic spectroscopic follow up is of paramount importance for three different reasons. First, to evaluate the accuracy and reliability of the Lyman-break selection technique that, albeit quite successful at $z \simeq 6$, has never been validated at these extreme redshifts. In addition, the intensity of the Ly α can provide clues on the rest frame properties of the observed galaxies: knowledge of the exact redshift and the contribution of Ly α and other emission lines to the observed broad-band magnitudes are needed to derive the rest-frame properties of the galaxies from the observed continuum (SFR, dust content, metallicity). Finally, and more intriguing, the very visibility of the Ly α and the distribution of its equivalent width in high- z galaxies can provide useful constraints on the ionization state of the intergalactic medium (IGM) at epochs less than 800 Myr

after the Big-Bang (e.g. Fontana et al. 2010, F10 in the following; Ouchi et al. 2010).

To date, only a few galaxies have been confirmed at $z \simeq 7$ or beyond. Following the early identification of the $z = 6.96$ Ly α emitter by Iye et al. (2006), a gamma ray burst host was reported at $z \simeq 8.1$ by both Salvaterra et al. (2009) and Tanvir et al. (2009), but with considerable uncertainties on the exact redshift, due to the absence of an emission line in the spectra. Very recently the detection of a galaxy at $z=8.6$ was claimed by Lehnert et al. (2010), although the Ly α emission line in the spectrum has very low S/N and a high uncertainty in the flux calibration.

In this context we have started a systematic campaign of spectroscopic follow-up of $z \simeq 7$ “z-band dropout” candidates, selected from our imaging survey obtained with VLT/Hawk-I (C10a and C10b). In F10 we presented the results on the sample selected in the GOODS-S field. Out of seven candidates observed, we tentatively detected only one weak Ly α emission line at $z = 6.97$. As discussed in that paper (see also Stark et al 2010), this very low fraction of confirmations is at odds with what is expected by extrapolating the $z = 5 - 6$ surveys which detect a much larger fraction of Ly α emitters.

Our survey has continued over the two other fields described in C10b. In this paper we present the only two objects with a clear Ly α line at $z \geq 7$ found in the entire survey, which are both detected in the BDF4 field (Lehnert & Bremer 2003). The results on the final sample with a full discussion of their implication is deferred to a forthcoming paper (Pentericci et al. in preparation).

All magnitudes are in the AB system, and we adopt

$H_0 = 70$ km/s/Mpc, $\Omega_M = 0.3$ and $\Omega_\Lambda = 0.7$.

2. TARGET SELECTION AND SPECTROSCOPIC OBSERVATIONS

The targets were selected according to the criteria described extensively in C10b: besides the three z -band dropout candidates listed in Table 3 of that paper, other slits were filled with less secure $z = 7$ candidates as well as i -band dropouts.

Observations were taken in service mode with the FORS2 spectrograph on the ESO Very Large Telescope, during July–August 2010. We used the 600Z holographic grating, that provides the highest sensitivity in the range 8000 – 10000Å with a spectral resolution $R \simeq 1390$ and a sampling of 1.6Å per pixel for a $1'' \times 12''$ slit. The data presented here come from the co-addition of 86 spectra of 665 seconds of integration each, on a single mask, for a total of 15.9 hr, with median seeing around 0.8''. Series of spectra were taken at two different positions, offset by 4'' (16 pixels) in the direction perpendicular to the dispersion.

Standard flat-fielding, bias subtraction and wavelength calibration have been applied as in Vanzella et al. (2009) and F10. The sky background has been subtracted between consecutive exposures, exploiting the fact that the target spectrum is offset due to dithering. Before combining frames, particular care has been devoted to the possible offset along the wavelength direction, by measuring the centroids of the sky lines in the wavelength interval 9400–9900Å. We have also carried out the sky subtraction by fitting a polynomial function to the background. The two approaches provide consistent results.

Finally, spectra were flux-calibrated using the observations of spectrophotometric standards. Slit losses are small, given the extremely compact size of the targets and have been neglected in the subsequent discussion.

3. RESULTS

3.1. Redshift determination

We detect a prominent emission line in the spectra of two galaxies, candidates $BDF - 521$ and $BDF - 3299$ (C10b), at wavelengths of 9735Å and 9858Å respectively. In Figures 1 and 2 we present the sky-subtracted extracted 1-dimensional spectra and 2-dimensional spectra for both objects. No other lines are detected in the rest of the spectra and no continuum is detected for either object. The total line fluxes are $1.6 \pm 0.16 \times 10^{-17} \text{ergs}^{-1} \text{cm}^{-2}$ and $1.2 \pm 0.14 \times 10^{-17} \text{ergs}^{-1} \text{cm}^{-2}$ respectively.

Both lines show a clear asymmetric profile with a sharp decline on the blue side and a prominent tail on the red side. This asymmetric profile, which we attribute to absorption by neutral hydrogen, is the best and in many cases unique diagnostic of high- z Ly α emission. Indeed most LAEs and LBGs at high redshift are too faint to detect the break in the continuum caused by IGM attenuation, with the exception of few very bright objects (Kodaira et al. 2003).

We have investigated the possibility that the lines are instead due to other features, such as H α , H β , [O III] λ 5007 or the doublet [O II] λ 3726 – 3729 in the spectra of lower redshift objects. If the detected emission lines were H β or [O III] λ 5007 at lower redshift ($z \sim 1.0$

and ~ 0.95), then both emission lines should be seen in the observed wavelength range. Actually the other component of the [O III] doublet (at λ 4959) should also be observed, although with lower S/N. No other lines are detected in the spectra. We also checked that the positions of the expected lines were not coincident with any bright skylines.

In case of H α emission from $z \sim 0.50$ galaxies, the rest-frame EW of the line would be exceeding 300Å, a value that is very rarely observed in star forming galaxies at low redshift (Salzer et al. 2005). Furthermore, we note that these objects would have a relatively bright continuum also at wavelengths below 1μ , and should therefore be observed in the deep R, I, z -bands, where instead we set very stringent upper limits for non-detection ($AB = 28 - 29$ depending on the band, see Table 1 of C10b).

Finally, in the case of [O II] emitters, the resolution of our spectra ($R=1390$) would be enough to distinguish the two components of the doublet, which at $z = 1.6$ are separated by 8Å. We searched for examples in our masks, and we do detect the [O II] doublet in two galaxies at $z \sim 1.6$, one at $z \sim 1.5$ and two at $z \leq 1.3$. In particular the two [O II] at $z \sim 1.6$ fall in the same wavelength region as the lines discussed here and have a lower flux compared to our candidates. In all cases we can clearly distinguish the two components: examples at redshift 1.3, 1.5 and 1.6 are shown in the inset of Figure 2 (top right). Furthermore, we note that typically the [O II] doublet even when unresolved produces an opposite asymmetry with respect to the Ly α shape, because the λ 3726Å component is often weaker than the λ 3729Å (see also Rhoads et al. 2003).

Since the correct identification of the line is a critical issue when no other spectral features are present, as mentioned above, the asymmetry can be used to distinguish high- z Ly α emission from foreground [O II], [O III], or H α emitters (see Stern et al. 2000). To test our ability to recognize asymmetric lines with the S/N of our spectra, we run Monte Carlo simulations by inserting two-dimensional lines of different shapes (Gaussian, truncated Gaussian with variable width, and [OII] doublet with variable ratio of the two components) in the original science frames at positions corresponding to the observed wavelengths, normalized to the flux of our lines. The frames have been matched in seeing and spectral resolution and reduced as the real ones. This was repeated for all slits where we have no signal detected. We find that an asymmetric line is always recognized as such if it has a width $> 150 \text{km/s}$, and that the [OII] doublet in the 1-D spectra is always resolved into two components.

We also calculated the weighted skewness S_w introduced by Shimasaku et al. (2006), to quantify the asymmetry of the two lines. Ly α emission produces always a positive S_w : they set a conservative value of $S_w > 3$ to distinguish LAEs from foreground emitters, although there could be also LAEs with $S_w < 3$. For our two galaxies we find $S_w > 5 - 8$ (depending on the wavelength's range assumed for the measurement), very similar to the average S_w of $z = 6.6$ LAEs $\langle S_w^{z=6.6} \rangle = 7.31 \pm 1.51 \text{Å}$.

We conclude that both lines can be safely identified with Ly α emission: this implies redshifts of 7.008 ± 0.002

and 7.109 ± 0.002 for BDF-521 and BDF-3299, respectively.

3.2. Continuum fluxes and spectral slopes

In the following we determine the correct UV continuum magnitudes and the Ly α equivalent widths for each object.

• **BDF-521:** Figure 1 (top panel) shows the relative position of the Ly α line and the two filters Y and z. The IGM opacity affects only 2.7% of the Y-band filter (<0.05 mag for a flat F_ν spectrum), therefore we neglect the IGM attenuation. The observed magnitude is $Y = 25.86 \pm 0.11$, corrected to $Y_{cont} = 26.31$ if the Ly α contribution is subtracted. We note that for this source there is also a 2-sigma detection at mag 28.00 ± 0.60 in the z-band which is consistent with the Ly α falling at the edge of the z-band filter. Assuming $Y_{cont} = 26.31$ the rest-frame Ly α equivalent width is 64_{-9}^{+10} Å (where the errors come from the line flux uncertainty).

• **BDF-3299:** The observed magnitude is $Y = 26.15 \pm 0.14$, corrected to $Y_{cont} = 26.58$ if Ly α is subtracted. However in this case the IGM attenuation affects 15% of the Y-band filter, absorbing completely the continuum blue-ward of the Ly α line (see Figure 1). Assuming conservatively a flat spectrum for the continuum, we derive $Y_{cont} = 26.40$ and a rest-frame Ly α equivalent width of 50_{-8}^{+11} Å.

Adopting these Ly α EWs we derived the slopes of the UV continuum, fitting to the broad-band photometry a set of simple models with flux scaling as $F_\lambda \propto \lambda^\beta$, which include also the Ly α emission and IGM absorption. We derive the best fit models and the relevant error analysis with a standard χ^2 minimization. The results are shown in Figure 3, where we plot the best-fitting solutions along with the error analysis (see insets). The best-fit slopes are remarkably steep, with $\beta = -3.7$ and -2.7 for BDF-521 and BDF-3299, respectively, similar to those recently claimed for z-band dropouts on the basis of new HST WFC3 data ($\beta < -2.5$, Bouwens et al. 2010b; Oesch et al. 2010; Bunker et al. 2010; Finkelstein et al. 2010). However, much shallower solutions with $\beta < -1.7$ and < -0.9 are still allowed at 1-sigma c.l. ($\Delta\chi^2 = 1$). Clearly, these results are mostly constrained by the non-detection in the J and in the K-band (see Table 1).

3.3. Implication for the stellar population

We have first explored whether these lines can be ascribed to AGN. From the non-detection of NV in the stacked spectrum we derive a 1σ lower limit on the $Ly\alpha/NV > 8$. This value is higher than the average ratio for QSOs but not unusual for weak narrow-line AGN found amongst LBGs (e.g. Steidel et al. 2002), so we cannot exclude this possibility. However we rely on the fact that AGN are much rarer than galaxies, and in the following we will assume that the objects are star forming galaxies.

At the redshifts derived above the implied luminosities for the Ly α lines are 9.3 and $7.3 \times 10^{42} \text{ergs}^{-1}$. We estimate the star formation rate (SFR) from the Ly α luminosity using the Kennicutt’s relation (Kennicutt 1998) with the case B recombination theory as $SFR = 9.1 \times L(Ly\alpha)$, with $L(Ly\alpha)$ in units of 10^{43}ergs^{-1} . We obtain

values around $7-9 M_\odot \text{yr}^{-1}$ (see Table 1): they represent lower limits since they are not corrected for absorption effects which depend on various parameters, including the neutral fraction of the IGM and the kinematic status of neutral hydrogen within the galaxies (e.g. Ahn 2004).

From the continuum luminosity we obtain $L(UV_{1275}) = 8.1 \times 10^{28}$ and $L(UV_{1260}) = 7.6 \times 10^{28} \text{ergs}^{-1} \text{Hz}^{-1}$. We convert luminosities into SFR using the Kennicutt relation for UV continuum, $SFR(UV) = 1.4 \times 10^{-28} L(UV)$. We determine the flux at 1500Å assuming the slope beta derived before. We obtain SFRs of $8.9 M_\odot \text{yr}^{-1}$ and $9.4 M_\odot \text{yr}^{-1}$ respectively, similar to those determined from the Ly α line. These values are obtained assuming no dust and the agreement of $SFR(UV)$ and $SFR(Ly\alpha)$ is consistent with this scenario. Using instead a global fit to the overall photometry with Bruzual & Charlot templates and a Calzetti (2000) attenuation law, we find best fit values for SFR that are in excellent agreement with the above determinations, and $E(B-V)=0$. The standard error analysis on these fits provides the limits one can place on the maximum SFR. Given the poor constraints on the J and K-bands, we find that for all models acceptable at 68% confidence level $E(B-V)$ is lower than 0.25-0.35, while the SFRs upper limits are $160 M_\odot \text{yr}^{-1}$ and $400 M_\odot \text{yr}^{-1}$, respectively, for the two objects, depending on the combination of age and metallicity. Note that the adoption of a Gallerani et al. (2010) attenuation curve would provide a SFR limit about 2 times lower.

4. DISCUSSION

With the spectroscopic identification of these two $z > 7$ galaxies we have moved closer to the epoch of reionization and may possibly be observing “re-ionizers” at work at the end of this process. While it is clearly impossible to draw any statistical result out of two objects only, we discuss here a few implications.

Recently, several authors have argued that the fraction of galaxies with large Ly α EW increases in the redshift range $4 < z < 6$ (e.g. Stark et al. 2010; Douglas et al. 2010; V09). The two emitters reported here with Ly α EW $\geq 50 \text{Å}$ seem to continue this trend. Indeed the fraction of z-band dropouts spectroscopically confirmed is much higher for this field (two out of three candidates observed), compared to the GOODS-south field (one out of seven candidates, F10).

Therefore the main results of F10, namely that the fraction of galaxies with Ly α EW exceeding 50Å seems to show a sharp decline from $z \sim 6$ to $z \sim 7$, thus reversing the increasing trend from $z \sim 4$ to $z \sim 6$, appears in conflict with the present observations.

However we anticipate that the result in F10 is confirmed by the analysis of the final sample that includes a third field (Pentericci et al. in preparation) and a much larger statistics. The present spectra indicate that there are considerable field to field variations and therefore solid conclusions can be drawn only from large samples.

Turning to the nature of these objects, one can determine whether they are able to ionize the IGM around them. Many models indeed predict that only intrinsically UV bright galaxies have enough photons to build reionized “bubbles” around them, on reasonably short

timescales (Dayal et al. 2008). Following Loeb et al. (2005) and assuming SFR of $10M_{\odot}yr^{-1}$ and age $100Myr$ we derive a maximum radius of the HII region of $R_{MAX} = 0.73(f_{esc})^{1/3}$ Mpc physical with f_{esc} the fraction of escaping ionizing photons. We are assuming isolated galaxies surrounded by a medium that is mostly neutral when they started to form stars ($z \sim 8$). In order for the Ly α to be transmitted the optical depth τ_{damp} to Ly α absorption at the galaxy redshift has to be less than one (Wyithe & Loeb 2005): this corresponds to a $R = 1.1$ Mpc. Therefore the radius we have derived would not be large enough even if a maximum $f_{esc} = 1$ is considered.

As already mentioned the intrinsic SFRs could be considerably higher: for the maximum SFR consistent with our photometry, the galaxies could ionize a large enough region if they had $f_{esc} > 0.1$. Such values of f_{esc} are not commonly observed in the $z \simeq 3$ Universe with few exceptions, such as the compact LBG at $z = 3.8$ recently reported by Vanzella et al. (2010) for which the Lyman continuum ($\lambda < 912\text{\AA}$) has been detected directly and whose non-ionizing features reveals $\beta = -2.1$, very weak interstellar absorption lines and absence of Ly α emission.

We stress that with the current depth of the near infrared observations, it is not possible to produce better constraints on the UV slopes, dust content and SFR. This issue could easily be solved with a modest investment of HST time, by obtaining deep Y, J and H-band WFC3 observations.

If the steep slopes and the dust-free scenarios are confirmed, then the galaxies do not have enough photons to ionize the surrounding HII regions. In such a case, the visibility of the Ly α line in these two objects implies the existence of additional ionizing sources, either galaxies and/or objects of different nature. It is intriguing to sur-

mise that the field-to-field variations in Ly α visibility we observe indicate that the reionization process was very inhomogeneous at these epochs. A possible reason is a clustering effect, particularly efficient since the first objects formed in highly biased regions (e.g. Furlanetto et al. 2006).

We point out that the two confirmed LBGs in the BDF field are at a physical distance from each other that is of the same order as the clustering length of LAEs at $z = 6.6$ $r_0 = 2 - 5h_{100}^{-1}Mpc$ (Ouchi et al. 2010) (they are separated by $6'$ in the plane of the sky corresponding to 1.9 Mpc and by 0.101 in redshift space corresponding to a proper distance of 4.4 Mpc). However there is no evidence of significant enhancement in the density of z-band dropouts in this field.

Another possible mechanism suggested by Wyithe & Loeb (2005) is related to a previous QSO activity, i.e., the HII regions generated by quasars remain as a fossil after the quasar activity ends, since the recombination time is longer than the Hubble time at the mean IGM density for $z < 8$.

These scenarios and their combinations can be tested only when a sizable sample of high- z sources are confirmed and their clustering and physical properties are determined.

Observations were carried out using the Very Large Telescope at the ESO Paranal Observatory under Programme IDs 085.A-0844, 283.A-5052 and 181.A-0717. We thank the anonymous referee for useful comments. We would like to thank P. Dayal and A. Ferrara for useful comments and discussion. We acknowledge financial contribution from the agreement ASI-INAF I/009/10/0.

REFERENCES

- Ahn, S.-H., 2004, ApJ, 601, 25
 Bouwens, R. J., Illingworth, G. D., Oesch, P. A., et al. 2010a, ApJ, 709, L133
 Bouwens, R. J., Illingworth, G. D., Oesch, P. A., et al. 2010b, ApJ, 708, L69
 Bunker, A., J., Wilkins, S., Ellis, R. S., Stark, D. P., Lorenzoni, S., Chiu, K., Lacy, M., Jarvis, M. J., Hickey, S., 2010, MNRAS, 409, 855
 Calzetti, Daniela, Armus, Lee, Bohlin, Ralph C., Kinney, Anne L., Koornneef, Jan, Storch-Bergmann, Thaisa, 2000, ApJ, 533, 682
 Castellano, M., Fontana, A., Boutsia, K., et al. 2010, A&A, 511, A20+ (C10)
 Castellano, M., Fontana, A., Paris, D., Grazian, A., Pentericci, L., Boutsia, K., Santini, P., Testa, V., Dickinson, M., Giavalisco, M., 2010, A&A, 524, 28 (C10b)
 Dayal, P., Ferrara, A., & Gallerani, S. 2008, MNRAS, 389, 1683
 Douglas, L. S., Bremer, M. N., Lehnert, M. D., Stanway, E. R., & Milvang-Jensen, B., 2010, MNRAS, 409, 1155
 Fontana, A., Vanzella, E., Pentericci, L., et al. 2010, ApJ, 725, 205
 Finkelstein, S., L., Papovich, C., Giavalisco, M., Reddy, N., A., Ferguson, H. C., Koekemoer, A. M., Dickinson, M., 2010, ApJ, 719, 1250
 Furlanetto, S. R., Zaldarriaga, M., Hernquist, L., 2006, MNRAS, 365, 1012
 Gallerani, S., Maiolino, R., Juarez, Y., Nagao, et al., 2010, A&A, 523, 85
 Hu, E. M., Cowie, L. L., Barger, A. J., et al., 2010, ApJ, 725, 394
 Iye, M., Ota, K., Kashikawa, N., et al. 2006, Nature, 443, 186
 Kennicutt, Robert C., Jr., 1998, ApJ, 498, 541
 Kodaira, K., Taniguchi, Y., Kashikawa, N., Kaifu, N., Ando, H., Karoji, H., Ajiki, M., Akiyama, M., Aoki, K., et al., 2003, PASJ, 55, 17
 Lehnert, M. D., & Bremer, M. 2003, ApJ, 593, 630
 Lehnert, M. D., et al. 2010, Nature, 467, 940
 Loeb, A., Barkana, R., Hernquist, L., 2005, ApJ, 620, 553
 McLure, R. J., Dunlop, J. S., Cirasuolo, M., et al. 2010, MNRAS, 403, 960
 Oesch, P. A., Bouwens, R. J., Illingworth, G. D., et al. 2010, ApJ, 709, L16
 Ota, K., Iye, M., Kashikawa, N., et al., 2010, ApJ, 722, 803
 Ouchi, M., Shimasaku, K., Furusawa, H., et al., 2010, ApJ, 723, 869
 Rhoads, J. E., et al. 2003, AJ, 125, 1006
 Salzer, J. J., Jangren, A., Gronwall, C., Werk, J. K., Chomiuk, L. B., Caperton, K. A., Melbourne, J., & McKinstry, K. 2005, AJ, 130, 2584
 Salvaterra, R., Della Valle, M., Campana, S., et al. 2009, Nature, 461, 1258
 Shimasaku, K., Kashikawa, N., Doi, M., Ly, C., Malkan, M. A., Matsuda, Y., Ouchi, M., Hayashino, T., Iye, M., et al., 2006, PASJ, 58, 313
 Stark, D. P., Ellis, R. S., Chiu, K., Ouchi, M., & Bunker, A., 2010, MNRAS, 408, 1628
 Steidel, C. C., Hunt, M. P., Shapley, A. E., Adelberger, K. L., Pettini, M., Dickinson, M., Giavalisco, M., 2002, ApJ, 576, 653
 Stern, D., Bunker, A., Spinrad, H., Dey, A., 2000, ApJ, 537, 73
 Tanvir, N. R., Fox, D. B., Levan, A. J., et al. 2009, Nature, 461, 1254
 Vanzella, E., Giavalisco, M., Dickinson, M., et al. 2009, ApJ, 695, 1163 (V09)

Vanzella, E., Giavalisco, M., Inoue, A. K., Nonino, M., et al.,
2010, ApJ, 725, 1011

Wyithe, J. S. B. & Loeb, A., 2005, ApJ, 625, 1

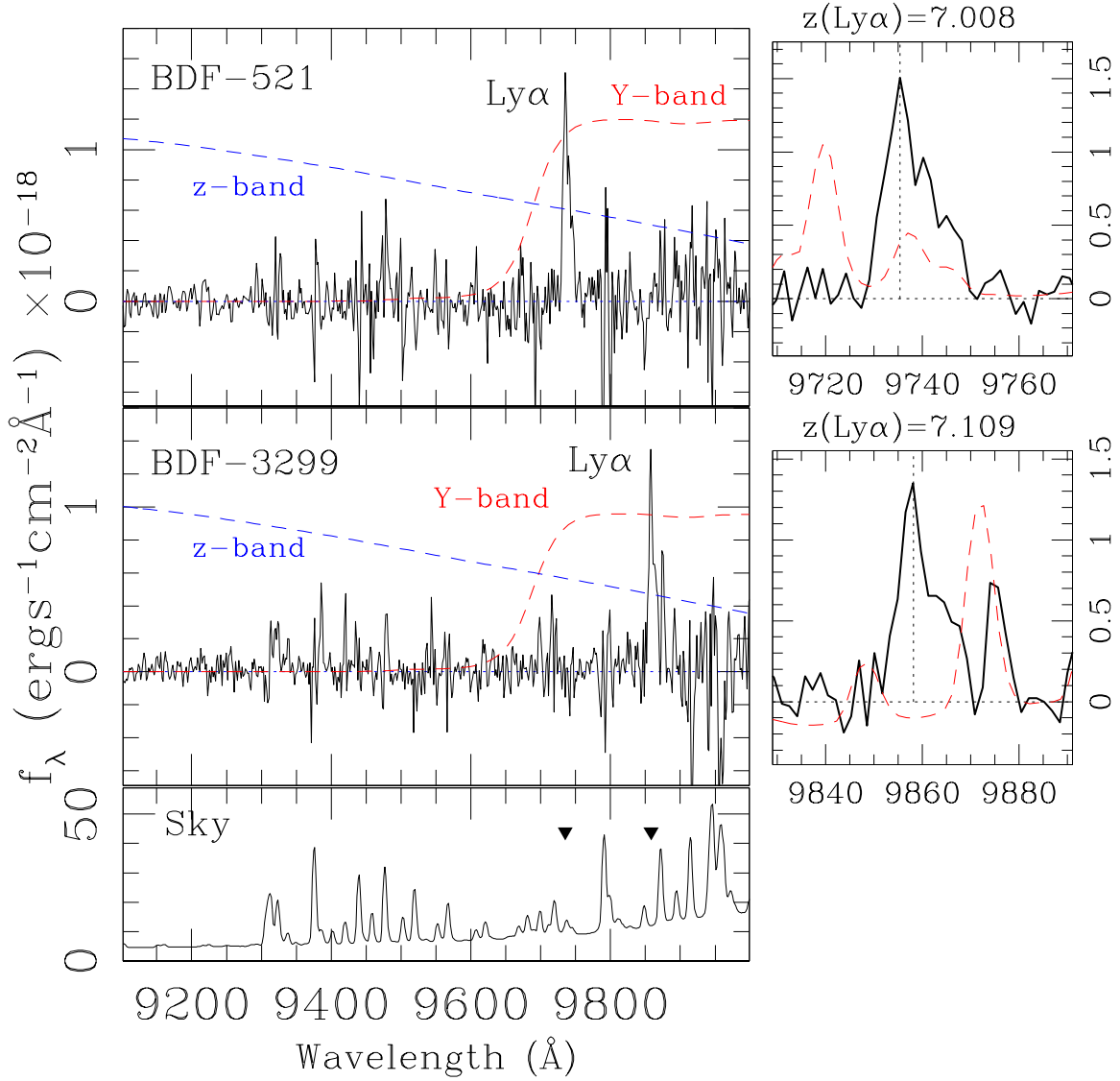


FIG. 1.— 1-dimensional spectra of candidates BDF-521 and BDF-3299. On the left panels spectra are shown with superimposed the z-band and Y-band filters. In the bottom the 1-dimensional (flux calibrated) spectrum of the sky is shown (the position of the Ly α lines are marked with triangles). On the right side the zoomed Ly α lines are shown with the position of the peak marked with a vertical dotted line. The two lines are significant at around 20 sigma level. In all panels units in the Y-axis are $10^{-18} \text{ erg s}^{-1} \text{ cm}^{-2} \text{ \AA}^{-1}$. The red dashed lines superimposed to the zoomed Ly α (on the right) show the spectrum of the sky in arbitrary units.

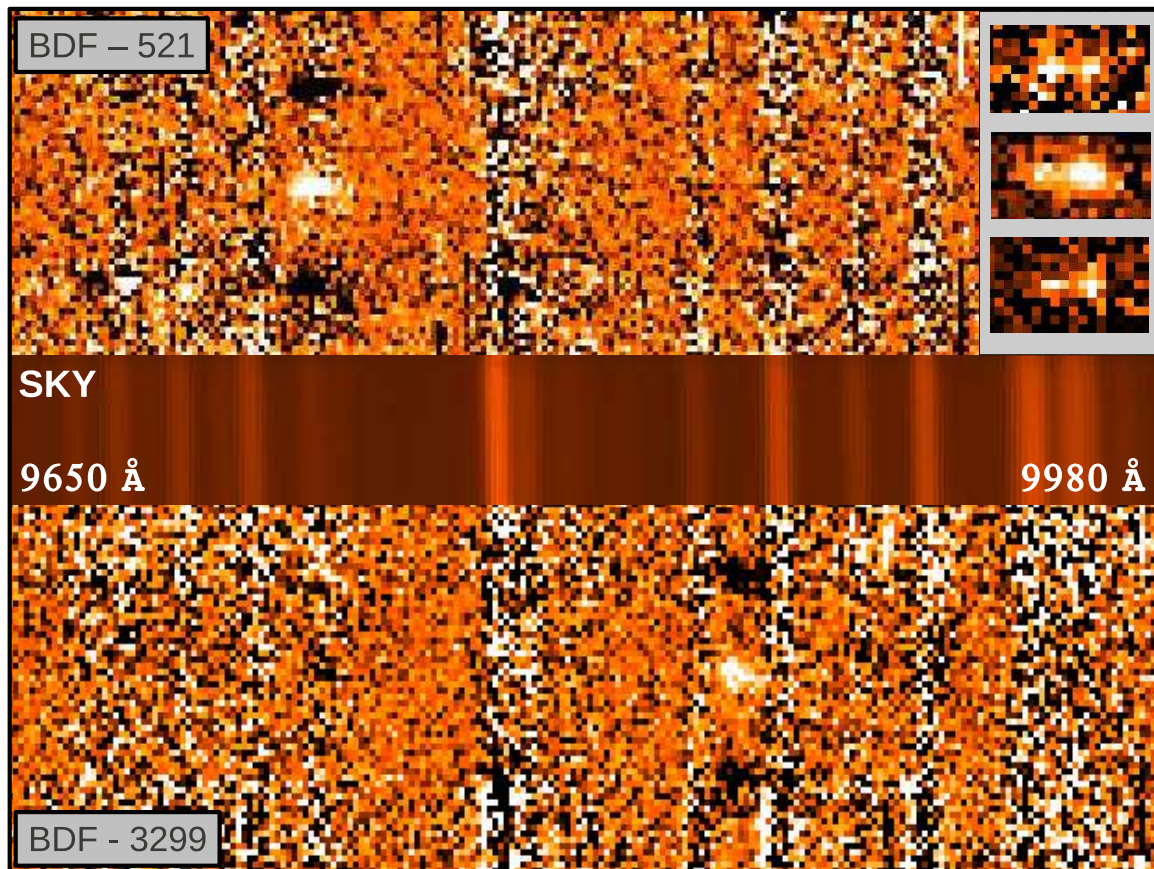


FIG. 2.— 2-dimensional sky subtracted spectra of BDF-521 (top) and BDF-3299 (bottom). In both cases the emission line is clearly detected. The “negative” features above and below the emission (typical of the sky subtraction technique) are also evident. In the middle the sky spectrum is shown as a reference for sky line positions. The resolved [O II] doublets at redshift 1.3, 1.5 and 1.6 are shown in the upper right corner, from bottom to top, respectively.

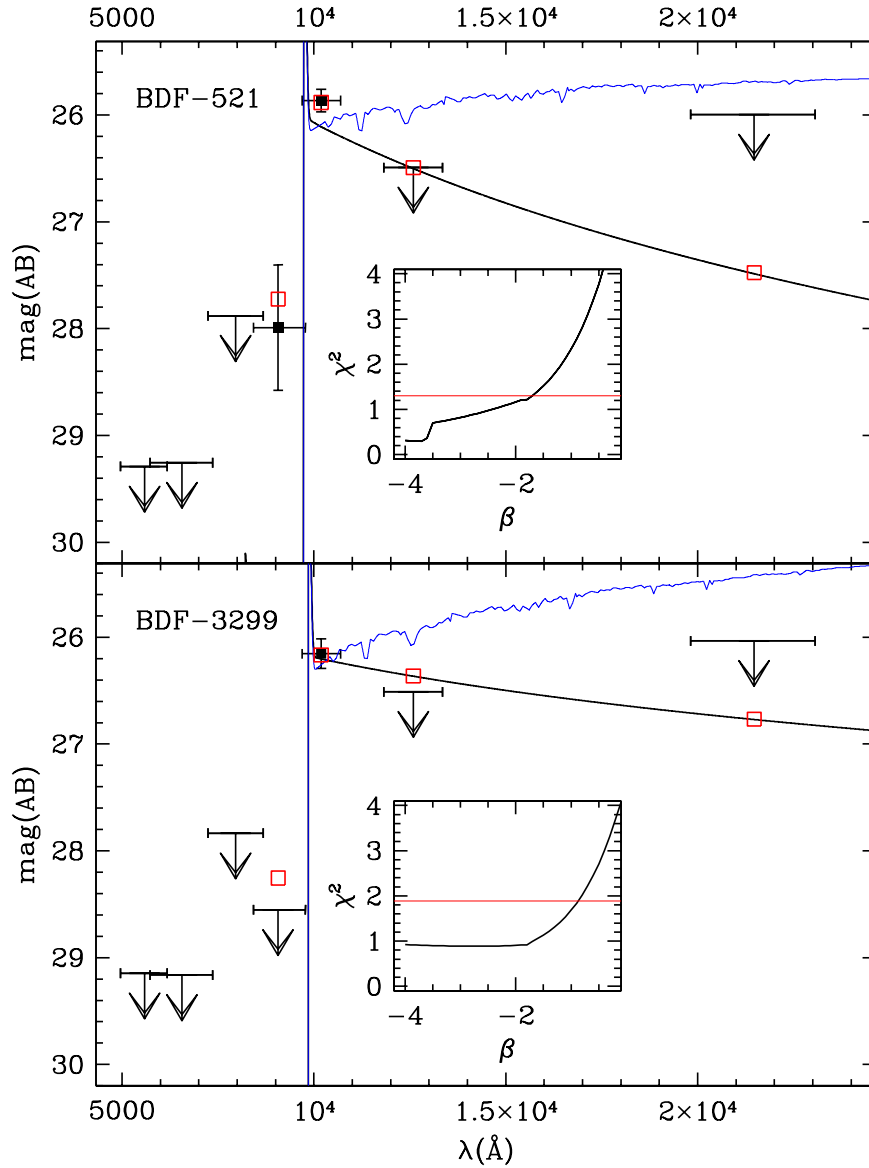


FIG. 3.— Observed photometry and best-fitting spectral model for BDF-521 (upper panel) and BDF-3299 (lower panel). Black dots and upper limits correspond to observed magnitudes. The solid line is a best-fitting β model. Red dots are the predicted magnitudes from the model. The blue thin line is the dust-extended Bruzual & Charlot model which provides the maximum SFR with an acceptable χ^2 . In the inset the χ^2 as a function of β is shown (the red horizontal line marks the $\Delta\chi^2 = 1$).

TABLE 1
SPECTROSCOPIC AND PHOTOMETRIC PROPERTIES OF THE TWO REDSHIFT SEVEN GALAXIES

ID	RA, DEC J2000	Redshift	$f(Ly\alpha)$	SFR($Ly\alpha$) $M_{\odot}yr^{-1}$	EW_{rest} \AA	FWHM ^a $km\,s^{-1}$	S_w \AA	z	Y	J 1σ	K 1σ
BDF-521	336.9444, -35.1188	7.008 ± 0.002	1.62 ± 0.16	8.5	64	240	8.2^{+2}_{-1}	28.00	25.86	>26.5	>26.0
BDF-3299	337.0511, -35.1665	7.109 ± 0.002	1.21 ± 0.14	6.6	50	200	> 5.9 ^b	>28.55	26.15	>26.5	>26.0

NOTE. — $f(Ly\alpha)$ in units of $10^{-17}ergs^{-1}cm^{-2}\text{\AA}^{-1}$. (a) Measured directly from the line and corrected for instrumental broadening. (b) This is considered a lower limit since the red side of the emission line is truncated by the presence of a bright skyline (see Figure 1).